Random-walk-based stochastic modeling of three-dimensional fiber systems

Hellen Altendorf[1,2,*] and Dominique Jeulin[2,†]

[1]*Department of Image Processing, Fraunhofer Institute of Industrial Mathematics, Fraunhofer-Platz 1, D-67663 Kaiserslautern, Germany*

[2]*Center of Mathematical Morphology, Mines Paris Tech, 35 rue Saint Honoré, F-77305 Fontainebleau Cedex, France*

(Received 20 July 2010; revised manuscript received 3 February 2011; published 28 April 2011)

For the simulation of fiber systems, there exist several stochastic models: systems of straight nonoverlapping fibers, systems of overlapping bending fibers, or fiber systems created by sedimentation. However, there is a lack of models providing dense, nonoverlapping fiber systems with a given random orientation distribution and a controllable level of bending. We introduce a new stochastic model in this paper that generalizes the force-biased packing approach to fibers represented as chains of balls. The starting configuration is modeled using random walks, where two parameters in the multivariate von Mises–Fisher orientation distribution control the bending. The points of the random walk are associated with a radius and the current orientation. The resulting chains of balls are interpreted as fibers. The final fiber configuration is obtained as an equilibrium between repulsion forces avoiding crossing fibers and recover forces ensuring the fiber structure. This approach provides high volume fractions up to 72.0075%.

DOI: 10.1103/PhysRevE.83.041804 PACS number(s): 81.05.Qk, 02.50.Ey

I. INTRODUCTION

The increasing interest in fibrous materials expands to a large variety of use cases. The most common fiber-reinforced polymers are currently contained in the enclosure of aircrafts, boats, and cars; furthermore, wound-disinfection tissues and thermal insulations make use of fibrous media. The macroscopic properties of these materials are highly influenced by the geometry of the fiber component, in particular by the direction distribution. Physical properties can be optimized by adapting the structural parameters appropriately. To this end, we need a realistic stochastic model for the geometry, including the main parameters for the fiber structure and taking into account the natural variability of the system.

In the area of stochastic geometry models, we distinguish between soft-core and hard-core systems. A hard-core system forbids overlap between the objects, which is strongly required, as such penetrations are not realistic in the case of solid glass or carbon fibers. Concerning random fiber systems, there exist several approaches providing either hard-core fiber systems with a low volume fraction, soft-core systems and sedimentation algorithms, providing hard-core systems with restrictions on the orientation distribution.

We recall in detail the state of the art in fiber modeling: The classical approach called the dilated Poisson line process was introduced in [1] and creates infinite straight cylinders in a soft-core network. Since then, fiber modeling has evolved into more flexible approaches. In order to achieve hard-core systems, the random sequential adsorption model was created in [2], which iteratively generates objects and tries to place them in the system such that they do not overlap with already-existing objects. This approach was applied for cylinders in [3]. Two other random fiber-packing methods have been developed: one for ellipsoids presented in [4] and one for spherocylinders in [5]. All three random packing approaches produce straight fibers in a hard-core system and achieve only low volume fractions of about 10%–15% for isotropic orientation distribution and a fiber aspect ratio of 10. For long fibers, as is the case for fiber-reinforced composites (aspect ratio of about 200), the producible volume fraction goes down to 5%, while 15%–55% is required. Furthermore, long fibers cannot be realized in a periodic window, as fibers tend to overlap themselves. Still, the periodic boundary condition is often required for simulations of physical properties.

There are also more physically motivated approaches of fiber sedimentation, which achieve, in general, high volume fractions but are limited in realizing a given orientation distribution. The fiber deposition model in [6] generates fibers oriented in the plane and deposes them with a certain bending parameter on the existing system. In this approach, high volume fractions can be achieved, but the most important parameter, the orientation distribution, is limited to the plane. The sequential deposition algorithm in [7] realizes a fall of random particles until they reach a local minimum of their potential energy. During the fall, rotation and displacement are not restricted. Therefore, the particle can change its orientation arbitrarily, and it cannot be assured that the desired orientation distributions will be achieved. This approach allows up to a 59% volume fraction for cylinders with an aspect ratio of 10.

Another hard-core bending fiber model was proposed in [8]. The representative volume element is divided into sublayers. Fibers are randomly oriented in the xy plane, and in the case of overlap, the newly added fiber changes the sublayer to avoid the existing fiber. The resulting chains of polyhedra with ellipsoid cross sections achieve a volume fraction of 35%–40%. Still, the buckled polyhedra do not appear to be very realistic, and again, the orientation distribution is restricted to the xy plane.

Moreover, soft-core bending fiber systems can be achieved by random walks introduced in [9] with the von Mises–Fisher distribution, controlling the smoothness of the bending. In this approach it is possible that long fibers bend to a circle; thus, the final orientation distribution cannot be controlled. The approach [10] provided 2D random walks with the multivariate von Mises–Fisher distribution, which also controls the deviation from the main fiber orientation, assuring a certain

*Hellen.Altendorf@mines-paristech.fr

†Dominique.Jeulin@mines-paristech.fr

loyalty to a given orientation distribution. Furthermore, in [11] a bending fiber model is proposed based on dilated cores made of curvature points connected by the spline interpolation. The last three models are soft-core systems.

The idea to represent fibers as chains of spheres was already considered in [12]. An irregular assembly of chains of tangent hard spheres (like in a pearl necklace) were studied to build dense packings with Monte Carlo simulation schemes. Hard-core configurations with low density are packed with a "box shrinkage" algorithm and relaxed in Monte Carlo algorithms by localized moves as flip, rotation, reptation, and intermolecular reptation. The aim of the approach in [12] is a highly dense packing, which was successfully achieved with a volume fraction of 63.9%, which corresponds to the densest packing of hard spheres. To this end, the restrictions on the fiber structure are very low, and thus, the approach is not suitable for reconstructing fiber-reinforced composites.

Material properties are highly influenced by the fiber structure, particularly its orientation distribution. This correlation is studied in [13–18]. Furthermore, Berhan and Sastry [19,20] studied the influence of model characteristics on percolation simulation for different high-aspect-fiber systems. In [19], the influence of soft-core and hard-core systems is examined, while [20] focuses on the waviness of the fibers. Berhan states that the frequently used straight and overlapping fiber systems are inappropriate to model fiber-reinforced materials, and he suggests using hard-core bending fiber systems. Those studies enhance the need for stochastic models, creating realistic fiber systems dedicated to fiber composite materials. In [21] and [22], we proposed quantification methods to analyze the most important characteristics of fiber systems. Now, a stochastic model is required to realize the measured properties. In contrast to physical simulations dedicated to systems of liquid crystals (e.g., [23]), we are only interested in the final configuration of the stochastic model and its properties, instead of the behavior of the fibers during the simulating process.

The aim of this paper is to provide a random hard-core fiber model with a controllable bending and high volume fractions. For this purpose, random walks are used to create a realistic system of bending fibers. The level of bending is controlled by two parameters in the multivariate von Mises–Fisher distribution. The created points are provided with a radius and the current orientation. The balls, defined by the points and the assigned radii, are connected in chains according to the paths of the random walks. This approach results in a soft-core system of bending fibers, modeled as chains of balls. In a second step, we apply a force-biased approach to achieve a hard-core configuration of the fiber system. Force-biased algorithms on spheres were introduced in [24] and statistically analyzed in [25]. The forces in our approach were inspired by the energy-reducing models known from molecular dynamics [24]. The mentioned forces describe the necessary displacement of the balls to relax the system. They do not act like mechanical forces. Two kinds of forces are applied to the ball centers: repulsion and recover forces. The repulsion force arises in the case of a fiber overlap and displaces the balls to a nonoverlapping position. The recover force maintains the fiber structure between the balls. It keeps the distance and the angles between a ball and its neighbors, allowing only a small deviation.

The approach works in a closed cubic window $W \subset \mathbb{R}^3$ with periodic boundary conditions. Overlap checks are effectively computed in subdivisions of the window W, where only neighboring cells need to be compared. Therefore, the algorithm has low computing time. We ensured the quality of the realization by evaluating the parameters of the final configuration.

Although ball chains are considered as the second type of ideal amorphous solids, they are purely used in modeling fibrous material. As stated in [26], in the case of nonoverlapping neighbor spheres, the maximal possible volume fraction rises up to the one of individual spheres: ≈ 0.64. With decreasing distance between neighboring spheres and increasing alignment of fibers, we approach a system of parallel cylinders. In this case, the problem reduces to a random packing of 2D disks, for which the maximal volume fraction can reach up to ≈ 0.78 [27]. In our approach, the distance between neighboring spheres is $\approx r/2$, where r is the sphere radius. This distance is one-quarter of the necessary distance for nonoverlapping neighbor spheres. Thus, the maximal possible volume fraction may lie between 0.64 and 0.78. As we include higher restrictions to the fiber structure as a random packing of tangent sphere chains [12], it is probable that we will not reach such high volume fractions for every set of parameters. Still, volume fractions around 50% were achieved for several input parameters. The maximal volume fraction of our experiments was 72.0075%, achieved for a z-axis preferred orientation distribution and an aspect ratio of 9.

II. METHOD

In this section, we describe the two main steps of the approach: the random walk and the force-biased fiber packing. We explain how the structural parameters of the fiber system are incorporated into the random walk and how we control the bending of the fibers. For the force-biased fiber packing, we introduce the repulsion and recover forces and explain how they are applied to the system. Furthermore, the stop criterion and the end step problem are discussed, and implementation details are given.

A. Random walk

Each fiber of the initial fiber system is modeled as a random walk. A random walk is a Markov process on $\mathbb{R}^3$ producing a chain of points. We assign to every point the current direction and a radius. The result of a random walk is a sequence of points in $\mathbb{R}^3 \times S^2 \times \mathbb{R}^+$, describing a fiber:

$$P = \{p_0, \ldots, p_l\}, \quad p_i = (x_i, \mu_i, r_i) \in \mathbb{R}^3 \times S^2 \times \mathbb{R}^+.$$

The starting point $p_0 = (x_0, \mu_0, r_0)$ and the path length l could be generated from four main distributions for the starting coordinate, the orientation, the radius, and the length. In general, the initial coordinate x_0 is uniformly distributed in a cubic window with periodic edge treatment $x_0 \sim U(W \subset \mathbb{R}^3)$.

The other three distributions describe the main parameters of the fiber system. For the orientation distribution, we have applied the β orientation (see [28] or [29]) with a global parameter $\beta \in \mathbb{R}^+ \backslash \{0\}$. For $\beta = 1$ it results in the uniform distribution on the sphere, for $\beta \to 0$ the distribution

concentrates on the z axis, and for $\beta \to \infty$ the orientations are distributed isotropically in the xy plane. The probability density function of the β orientation distribution is

$$p(\theta,\phi|\beta) = \frac{\beta \sin\theta}{4\pi[1+(\beta^2-1)\cos^2\theta]^{3/2}},$$

where (θ,ϕ) are the polar coordinates of the orientation $\mu_0 \in S^2$.

The radius and length can be simulated from any distribution on $\mathbb{R}^+$. The radius can either be fixed for the whole system or chosen once for each fiber or for every point during the random walk with some strategy for smooth variation. The number of fibers for the system is chosen depending on the required volume fraction. The fourth main characteristic of the fiber system, the bending of the fibers, is indirectly controlled by two parameters, κ_1 and κ_2, in the multivariate von Mises–Fisher distribution.

During the random walk, the generation of a new point p_{i+1} requires three steps: First, the new orientation μ_{i+1} is generated according to the multivariate von Mises–Fisher distribution, with the last orientation μ_i and the main fiber orientation μ_0 as parameters. Second, the new radius r_{i+1} is generated. Finally, the new coordinate is calculated as $x_{i+1} = x_i + \frac{r_{i+1}}{2}\mu_{i+1}$. The distance between the points is a trade-off between a representative fiber structure and a treatable number of points.

In [10] the multivariate von Mises–Fisher distribution is introduced for the 2D case. In 3D the corresponding probability density function is defined as

$$f(x|x_1,\kappa_1,x_2,\kappa_2) = c(x_1,\kappa_1,x_2,\kappa_2)\, e^{\kappa_1 x_1^T x + \kappa_2 x_2^T x},$$

where $x_1,x_2 \in S^{d-1}$ are two preferred directions and $\kappa_1,\kappa_2 \in \mathbb{R}^+$ are the reliability parameters toward the preferred directions. The factor $c(x_1,\kappa_1,x_2,\kappa_2)$ serves for the normalization, such that the integral over S^2 is equal to 1.

A useful observation is that every multivariate von Mises–Fisher distribution can be written as a classical von Mises–Fisher distribution with the parameters

$$\kappa = |\kappa_1 x_1 + \kappa_2 x_2|, \quad x_0 = \frac{\kappa_1 x_1 + \kappa_2 x_2}{\kappa},$$

which can be easily checked by inserting those parameters in the classical von Mises–Fisher density function. This simplifies the generation of the pseudorandom variables to the standard case, which is well described in [30]. Furthermore, this defines the normalization factor

$$c(\kappa) = \frac{\kappa}{2\pi(e^{\kappa} - e^{-\kappa})}$$
$$\Rightarrow c(x_1,\kappa_1,x_2,\kappa_2) = \frac{|\kappa_1 x_1 + \kappa_2 x_2|}{2\pi(e^{|\kappa_1 x_1 + \kappa_2 x_2|} - e^{-|\kappa_1 x_1 + \kappa_2 x_2|})}.$$

In our approach, the first preferred direction is the main fiber orientation μ_0, and the second preferred direction is the orientation of the previous point μ_{i-1}. Therefore, κ_1 describes the reliability to the main fiber orientation, whereas κ_2 describes the reliability to the last orientation and hence specifies the smoothness of the bending. The probability density function for the ith step in the random walk (with $i \geqslant 1$) is

$$f(\mu_i|\mu_0,\kappa_1,\mu_{i-1},\kappa_2) = c(\mu_0,\kappa_1,\mu_{i-1},\kappa_2)\, e^{\kappa_1 \mu_0^T \mu_i + \kappa_2 \mu_{i-1}^T \mu_i}.$$

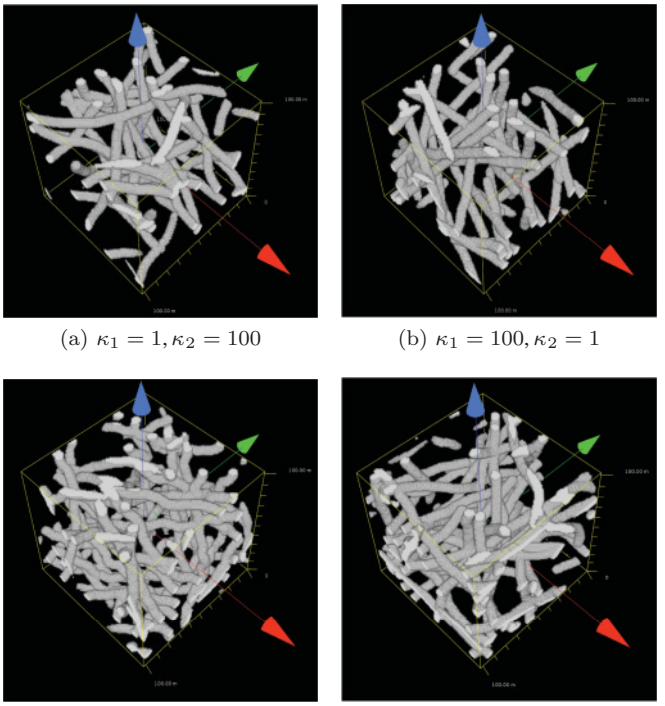

(a) $\kappa_1 = 1, \kappa_2 = 100$ (b) $\kappa_1 = 100, \kappa_2 = 1$

(c) $\kappa_1 = 10, \kappa_2 = 10$ (d) $\kappa_1 = 10, \kappa_2 = 100$

FIG. 1. (Color online) Realizations of the fiber model created by random walks. Common parameters are as follows: number of fibers $n = 10$, window side length $s = 100$, fixed fiber length $l = 300$, fixed fiber radius $r = 3$, and isotropic orientation distribution ($\beta = 1$).

Realizations of the soft-core fiber model created by random walks with varying choices of reliability parameters κ_1 and κ_2 are shown in Fig. 1.

The mean fiber orientation of a created ball chain $P = \{p_0,\ldots,p_l\}$ is defined as $\bar{\mu}(P) = \frac{p_l - p_0}{|p_l - p_0|} \in S^2$. The mean orientations of the created fibers are supposed to be realizations of a global orientation distribution for the fiber system. The starting orientations μ_0 are chosen with respect to the global orientation distribution, but the mean orientation differs from μ_0 with a deviation according to the reliability parameters κ_1 and κ_2. To ensure the global orientation distribution, we rotate the chosen fiber, so that the mean fiber orientation equals the originally chosen main fiber orientation: $\bar{\mu}(P) = \mu_0$. The fiber structure (length, radii, bending) remains constant during the rotation.

Every ball $p_i = (x_i,\mu_i,r_i)$ is adjusted to $p_i = (x_i',\mu_i',r_i)$ with

$$x_i' = x_0 + \mathrm{Rot}(x_i - x_0, n, \alpha),$$
$$\mu_i' = \mathrm{Rot}(\mu_i, n, \alpha),$$
$$n = \mu_0 \times \bar{\mu}(P),$$
$$\alpha = \measuredangle(\mu_0, \bar{\mu}(P)),$$
$$\mathrm{Rot}(\mu,n,\alpha) = (n\cdot\mu)n + \cos\alpha((n\times\mu)\times n) + \sin\alpha(n\times\mu),$$

where a center dot ($\cdot$) notates the scalar product (or inner vector product) and a times sign ($\times$) indicates the cross product (or vector product). The random walks create a stochastic fiber

model made of overlapping ball chains. The system is defined by the graph (P,E), where

$$P = \{p_{1,1}, p_{1,2}, \ldots, p_{1,l_1}, p_{2,1}, \ldots, p_{n,l_n}\} \subset \mathbb{R}^3 \times S^2 \times \mathbb{R}^+$$

yields the created points and

$$E = \{(p_{i,j}, p_{i,j+1}) \mid i \in \{1,\ldots,n\}, j \in \{1,\ldots,l_i\}\}$$

yields the connections between the points according to the n paths of the random walks. l_i is the number of points for the ith fiber. Furthermore, we define

$$C = \{(q,p,q') \in P^3 \mid (q,p) \in E \wedge (p,q') \in E\}$$

as the joints between two edges. For further steps, we need to remember the original distance between two neighboring points and the original angle in every joint. Thus, we define an original distance and an original angle function,

$$\begin{array}{rccc} D_{\text{orig}}: & E & \to & \mathbb{R}^+ \\ & (p,q) & \to & |x_p - x_q| \\ A_{\text{orig}}: & C & \to & [0,\pi] \\ & (q,p,q') & \to & \measuredangle(x_q,x_p,x_q'), \end{array}$$

and fix the mappings before the fiber packing process starts.

B. Force-biased fiber packing

To achieve a hard-core fiber system, the fiber packing applies two kinds of forces to the ball centers given from the soft-core fiber model: the repulsion force to separate overlapping balls and the recover force to keep the fiber structure between the balls. The reconfiguration of the ball chains is realized in several steps. In each step, the forces are calculated for the current configuration of the system, and displacements are performed.

1. Repulsion force

The repulsion force for a pair of overlapping balls describes the necessary displacement to make them nonpenetrating. The overlap between two balls is permitted if the balls are close neighbors in the same fiber. In this case, we define the two points $p,q \in P$ as related:

$$p \sim q \Leftrightarrow \exists \text{ path between } p \text{ and } q \text{ with length} \leqslant 5. \quad (1)$$

The value of 5 is an approximation for the minimal distance of two balls in the same chain that do not naturally overlap. The distance between the ball centers of two direct neighboring balls is chosen as $r/2$. In this case, balls in the same chain connected by a path with length less than 4 do overlap naturally. According to small deviations in the radius or additional curvature, we increase the minimal path length to 5.

Let $p_1 = (x_1,d_1,r_1), p_2 = (x_2,d_2,r_2) \in P$ be two arbitrary points in the fiber system. The overlap between those two points is

$$\text{Overlap}(p_1,p_2) = \max[0, r_1 + r_2 - d(x_1,x_2)],$$

with the distance function $d(x_1,x_2)$ respecting the periodic edge treatment. The repulsion force is

$$F_{rp}(p_1,p_2) = \mathbb{1}_{p_1 \sim p_2} \frac{\text{Overlap}(p_1,p_2)}{2} \frac{x_1 - x_2}{|x_1 - x_2|},$$

and it is applied if the points are not related as defined in equation (1). The force on p_1 works in the opposite direction to p_2, with a strength linearly dependent on the overlap. The total repulsion force for point p_1 is cumulated over all points in P:

$$F_{rp}(p_1) = \sum_{q \in P} F_{rp}(p_1,q).$$

2. Recover force

The recover force keeps the distance between neighboring points by modeling springlike forces between them, and it keeps the angle in the joints by modeling open springs between the connections. Open springs describe the fact that there is a force for decreasing but none for increasing angles. Thus, a fiber can be straightened but not folded into a clew.

The recover force is induced by a displacement of the original ball coordinate as an effect of the applied repulsion force. By applying the recover forces to one ball it induces recover forces on its neighbors. Even if the strength of the indicated forces is decreasing, a kind of domino effect has started, and the process becomes infinite. In order to stabilize the movement, we introduce a smoothing factor, which acts like friction. We define a minimal change x_s, which is necessary to induce a force, and a change x_e when the force regains its full strength. The friction factor is defined as

$$f_{x_s,x_e}(x) = \begin{cases} 0 & x < x_s, \\ \frac{1}{2} - \frac{1}{2}\cos\left(\frac{|x|-x_s}{x_e-x_s}\pi\right) & x_s \leqslant x \leqslant x_e, \\ 1 & x_e < x. \end{cases}$$

The curve $f_{x_s,x_e}(x)$ is given in Fig. 2.

a. Spring force. In order to keep the distances between the balls in a fiber, we define a force between the centers of the balls, with a strength linearly dependent on the change of distance. This kind of force can be interpreted as a spring between the ball centers. Let $p = (x_p,d_p,r_p)$ and $q = (x_q,d_q,r_q)$ be two neighboring points. The change of distance is

$$\Delta D(q,p) = D_{\text{orig}}(q,p) - |x_q - x_p|,$$

and the unit vector for the direction of the force is

$$v(p,q) = \frac{x_p - x_q}{|x_p - x_q|}.$$

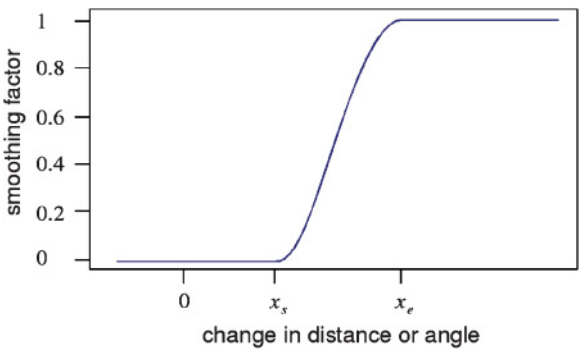

FIG. 2. (Color online) Friction factor for recover forces.

Thus, the recovery spring force F_{rs} on a point p is defined as

$$F_{rs}(p) = \sum_{q\in P}\left\{[\mathbb{1}_E(p,q)+\mathbb{1}_E(q,p)]f_{d_s,d_e}\left(\frac{|\Delta D(q,p)|}{D_{\text{orig}}(q,p)}\right)\right.$$
$$\left.\times[\Delta D(q,p)]v(p,q)\right\}.$$

The spring force is applied to p for every direct neighbor (at most two). It is linear to the distance change and multiplied by the friction factor on the ratio of distance change. For the realizations created in this paper, the friction parameters were chosen as $d_s = 5\%$ and $d_e = 10\%$.

b. Angle force. In order to keep the angle between joints, we define a recover force on each point having two direct neighbors. Let $(q_1,p,q_2) \in C$ be a joint in the point $p = (x,d,r)$ with the neighbors $q_1 = (x_1,d_1,r_1)$ and $q_2 = (x_2,d_2,r_2)$. We define

$$\alpha_0 = A_{\text{orig}}(q_1,p,q_2),$$
$$m = \overline{x_1x_2} \cap \text{Plane}[x,\perp(x_1-x_2)],$$
$$h_1 = |m-x_1|, \quad h_2 = |m-x_2|, z = |m-p|,$$
$$\alpha_1 = \tan^{-1}(h_1/z), \quad \alpha_2 = \tan^{-1}(h_2/z),$$
$$\tan\alpha = \tan(\alpha_1+\alpha_2) = \frac{z(h_1+h_2)}{z^2-h_1h_2},$$
$$z_0 = \frac{h_1+h_2+\sqrt{(h_1+h_2)^2+4h_1h_2\tan^2\alpha}}{2\tan\alpha}.$$

Now, the recovery angle force F_{ry} on a point p is defined as

$$F_{ra}(p) = \mathbb{1}_{\exists q_1,q_2\in P,(q_1,p,q_2)\in C}\ f_{\alpha_s,\alpha_e}(\alpha_0-\alpha)\,(z-z_0)v(m,p).$$

The angle force is linearly dependent on the necessary displacement to regain the original angle, and it is multiplied by the friction factor, depending on the angle change. For the realizations created in this paper, the friction parameters were chosen as $\alpha_s = 0.1^\circ$ and $\alpha_e = 0.2^\circ$. The geometrical construction is visualized in Fig. 3.

3. *Application of force*

The total force on an arbitrary point $p \in P$ is composed of the sum of all mentioned forces:

$$F_{\text{total}}(p) = \sum_{q\in P} F_{rp}(p,q) + \rho F_{rs}(p) + \rho F_{ra}(p),$$

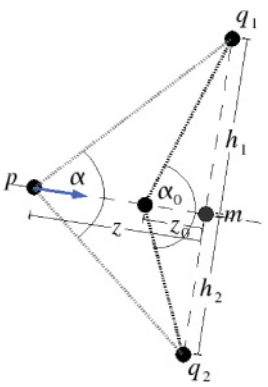

FIG. 3. (Color online) Geometry for angle force.

where ρ is a factor in $[0,1]$ leading to a smooth development of the recover forces, favoring the repulsion forces in the first steps. For the realizations created in this paper, we chose $\rho = 0.2$. In order to limit the possible displacement of a point, we define an upper bound $F_{\max}$ for the final force strength:

$$F_{\text{final}}(p) = \frac{F_{\text{total}}(p)}{|F_{\text{total}}(p)|}\min(|F_{\text{total}}(p)|, F_{\max}).$$

In each step, the ball center of p is displaced by the limited final force:

$$x'_p = x_p + F_{\text{final}}(p).$$

After the displacement in a step, the forces are recalculated for the new configuration and applied in a following step.

C. Stop criterion and end step

During the packing process the forces decrease very quickly in the beginning and converge slowly to zero in the end. The process should be stopped by a criterion dependent on the force strength. In our implementation, the algorithm terminates with a solution if the total force strength $\sum_{p\in P} F_{\text{total}}(p)$ falls below a certain limit and the displacements become negligible. For the realizations created in this paper, we chose the limit as $0.002sn$, where n is the number of fibers and s the side length of the window. That means the mean sum of necessary displacements in a fiber is smaller than 0.2% of a unit size. When the volume fraction is chosen too high, it is possible that there is no configuration with low force strength. In this case, the process will not converge, and we need to add a stop criterion. We have chosen an upper bound for the number of steps of 10 000. If the process reaches this limit, it will terminate unsuccessfully.

In the case of a successfully completed process, the total force strength is negligible. Still, one should be aware that the total force on a point is a sum of different forces. Thus, even if the sum of forces is zero, it is not certain that every specific force is negligible in its strength. Regarding the repulsion force as specific force, it may happen that the recover force acts in the opposite direction with exactly the same strength [as shown in Fig. 4(a)]. As the repulsion force is linear to the overlap, we conclude that the fiber packing does not necessarily have a zero overlap, which means that the system may not be totally hard core.

This effect is similar to the maximal random jammed state, known from random packings (see [26]). In our approach, a ball is never jammed as its displacement is defined by reducing forces and overlap in a following configuration is not strictly forbidden. Still, we have a similar situation if the requested volume fraction is too high for the fiber structure.

To assure a nonoverlapping system, we accept an outcome only if the maximal overlap falls below a certain limit. Here we chose $0.1r_{\min}$, where $r_{\min}$ is the minimal radius in the system. Then, a final step is added, where the radius of each point is reduced according to the maximal overlap with other points. This approach is similar to the idea in the force-biased sphere packing. Let $p = (x,d,r) \in P$ be an arbitrary point of the fiber system; the radius r is reduced to

$$r' = r - \tfrac{1}{2}\max_{q\in P, q\sim p}\text{Overlap}(p,q).$$

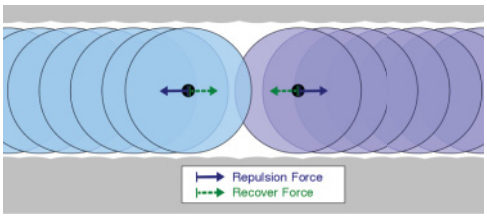

(a) Trade-off between repulsion and recover forces.

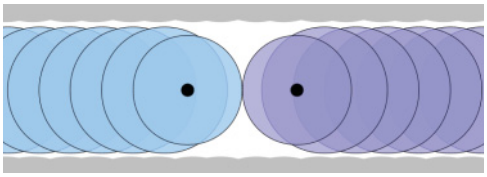

(b) Solution 1: Reducing the radius.

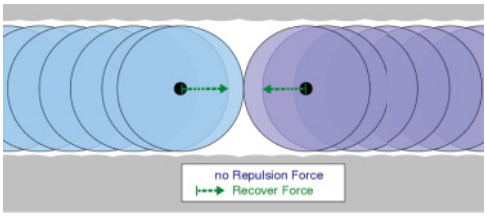

(c) Solution 2: Endstep regarding only the repulsion forces.

FIG. 4. (Color online) Trade-off problem in the final configuration with two possible solutions: reducing the radius or applying an end step considering only the repulsion forces. Note that force vectors are elongated for visualization reasons; they do not correspond to the necessary displacements.

If the accuracy of the radius distribution is very important, the end step can be replaced by a second round of the packing algorithm, where only the repulsion force is active. In this case, the theoretical recover force strength should be checked afterward, to make sure that the fibers are not drawn apart.

D. Implementation details

The periodic distance function for $x = (x_x, x_y, x_z)^T$ and $y = (y_x, y_y, y_z)^T$ and a window $W = [0, w_x] \times [0, w_y] \times [0, w_z]$ is defined as

$$d(x,y) = \left| \begin{pmatrix} \min(|x_x - y_x|, w_x - |x_x - y_x|) \\ \min(|x_y - y_y|, w_y - |x_y - y_y|) \\ \min(|x_z - y_z|, w_z - |x_z - y_z|) \end{pmatrix} \right|.$$

The repulsion force on an arbitrary point $p \in P$ is defined as the sum over all points $q \in P$. Still, the repulsion force is equal to zero if balls p and q are not overlapping, which is definitely the case if $q \notin B_{r_p + r_{\max}}(x_p)$, where $r_{\max} = \max_{q \in P} r_q$. As proposed in [24], we divide the window W into smaller cubic subwindows with a side length $s_i \geqslant r_{\max}$ with $i \in \{x, y, z\}$. For a window $W = [0, w_x] \times [0, w_y] \times [0, w_z]$ the side lengths of the subwindow are calculated as

$$s_i = \frac{w_i}{n_i}, \quad n_i = \lceil \frac{w_i}{r_{\max}} \rceil.$$

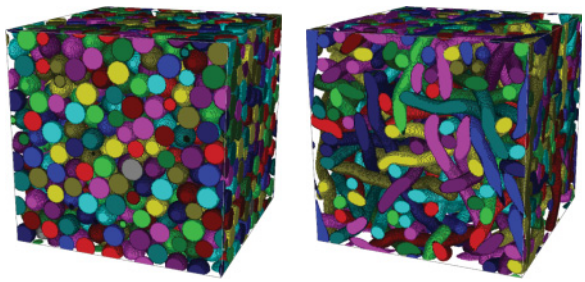

(a) $\chi = 1$, $n = 1146$, $V_V = 57.27\%$

(b) $\chi = 33$, $n = 90$, $V_V = 50.35\%$, isotropic orientation ($\beta = 1$)

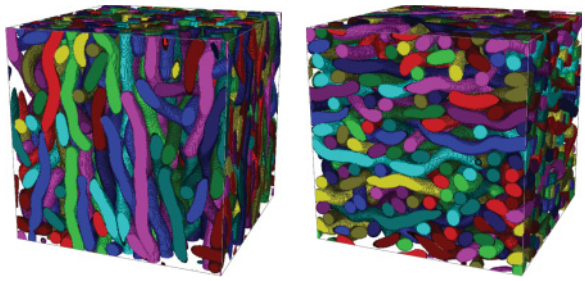

(c) $\chi = 17.67$, $n = 170$, $V_V = 49.60\%$, orientation in z-direction ($\beta = 0.1$)

(d) $\chi = 17.67$, $n = 170$, $V_V = 49.95\%$, orientation in xy-plane ($\beta = 10$)

FIG. 5. (Color online) Realizations for packed fiber systems. Common parameters are as follows: window side length $s = 100$ and bending parameters $\kappa_1 = 10$ and $\kappa_2 = 100$.

Thus, $B_{r_p + r_{\max}}(x_p)$ is included in the union of the subwindow including p and its neighboring subwindows. The overlap check is limited to this union.

III. RESULTS

Figure 5 shows realizations of the presented model with varying input parameters for the fiber aspect ratio χ, the number of objects n, and the main orientation distribution. The parameters and the achieved volume fraction V_V are given below each realization.

The aspect ratio is generally defined as length divided by diameter. In the case of a ball chain $p_1, \ldots, p_n$ with fixed radius r, the aspect ratio χ can be calculated as

$$\chi = \frac{2r + \sum_{i=1}^{n-1} |p_i - p_{i+1}|}{2r}.$$

To evaluate if the final configuration fulfills the required distributions, we observed the changes in the characteristics of the fiber system during the force-biased packing for three realizations with different choices of $\beta \in \{0.1, 1, 10\}$. The remaining parameters are chosen as follows: window size $= 100^3$, length $= 50$, radius $= 5$, number of fibers $= 100$, and required density $= 44.483\%$. The evolution of the characteristics is shown in Fig. 6. The estimation of length and radius is obvious. The measured density is the volume fraction of the discretized image. The β estimate is the numerical approximation of the maximal likelihood estimator, which cannot be resolved theoretically. The estimation of the bending parameters κ_1 and κ_2 is not that simple, but experiments

showed that they can be approximated for $\kappa_2/\kappa_1 > 2$ with the following estimates:

$$\hat{\kappa}_1 = 1/\mathrm{Var}_1,$$
$$\hat{\kappa}_2 = 2/\mathrm{Var}_2,$$
$$\mathrm{Var}_1 = \frac{1}{n}\sum_{j=1}^{n}\left(\frac{1}{l_j}\sum_{i=0}^{l_j}\left[\mu_{j,i} - \bar{\mu}\left(p_{j,1},\ldots,p_{j,l_j}\right)\right]^2\right),$$
$$\mathrm{Var}_2 = \frac{1}{n}\sum_{j=1}^{n}\left(\frac{1}{l_j - 1}\sum_{i=0}^{l_j-1}(\mu_{j,i} - \mu_{j,i+1})^2\right).$$

Even if the estimators for κ_1 and κ_2 are not highly accurate, they are still measures for the global and local bending. As long as the measures of the real data set and the measures of the final model configuration are close, the aim of realistically reproducing the fiber structure is fulfilled.

In Fig. 6, the first steps are mostly driven by the repulsion forces, which evokes changes in the local structure and therefore in the parameter measure. When the repulsion force decreases, the recover forces reconstruct the fiber structure, which results in a convergence of the measures to the requested values. Most measures start with the requested values, except for the density and the global bending parameter κ_1. The low density in the beginning is evident, as the overlapping fiber volume is counted only once. The deviation of the global bending parameter κ_1 or reliability to the mean fiber orientation is caused by the different measure condition. During the realization of the fiber structure, κ_1 represents the reliability to the chosen fiber orientation μ_0, whereas the measure of κ_1 reflects the reliability to the actual mean fiber orientation $\bar{\mu}(P)$, which is slightly too high. The convergence to the required value of κ_1 is surprisingly good and is probably caused by the trade-off between the recover force to the original fiber structure and the tolerance range of local deviation.

We stress once more that the important configuration is the final one, and the geometric characteristics during the process are studied to understand better what happens during the packing process. The evaluation of the quality of our models is only based on the geometric characteristics of the final configuration, as shown in Table I.

In both visualizations, we can see that the parameters of length, radius, and density fit perfectly to the requested values. The global and local bending κ_1 and κ_2 are approaching the required values, as expected. As the local orientations have some tolerance during the packing process, it is understandable that the final bending values are lower than the initial ones. If one is not satisfied with the final values for bending, there

TABLE I. Parameter measures for the final configuration of experiments from Fig. 6.

	Density	Length	Radius	κ_1	κ_2	β
Required	44.48%	50	5	10	100	various
$\beta = 0.1$	43.94%	50.66	4.99	9.91	96.32	0.134
$\beta = 1$	43.90%	50.75	4.98	8.21	80.95	0.87
$\beta = 10$	44.10%	50.90	4.98	8.03	82.39	5.6

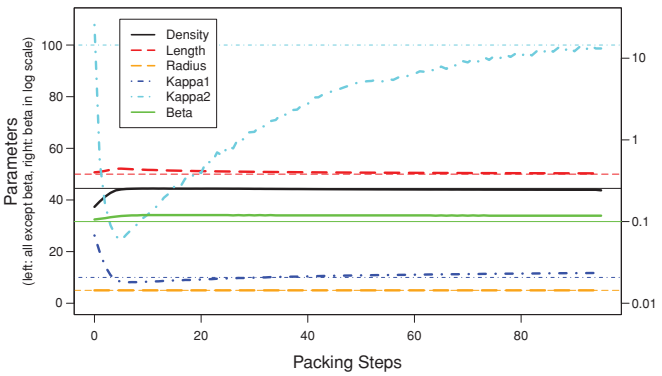

(a) Orientation distribution with $\beta = 0.1$

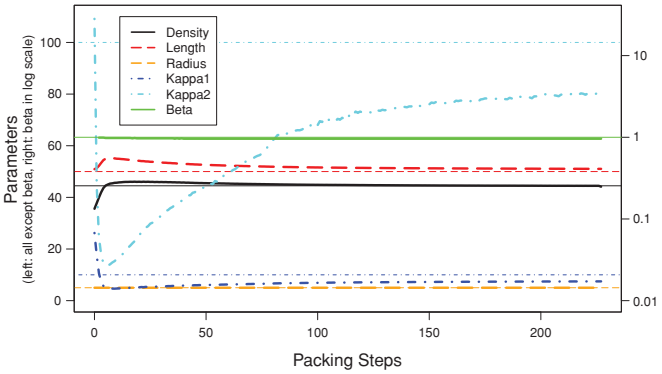

(b) Orientation distribution with $\beta = 1$

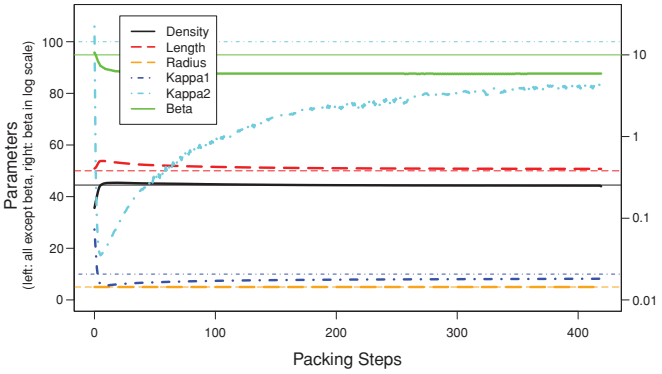

(c) Orientation distribution with $\beta = 10$

FIG. 6. (Color online) Evolution of estimated model parameters during the packing process for different choices of β for the orientation distribution. Fixed parameters are as follows: window size $= 100^3$, length $= 50$, radius $= 5$, number of fibers $= 100$, and starting density $= 44.483\%$.

are two possibilities to improve this: first, one can choose the initial values higher than required, and second, one can reduce the tolerance α_s and α_e in the packing process. The parameter β for the orientation distribution is acceptably approximated for the choices $\beta = 0.1$ and $\beta = 1$, whereas the girdle orientation with $\beta = 10$ could not be maintained that strictly during the packing process. The results would even become worse for higher choices of β. With the described model, we can realize parameters in the range of 0.05–5. If a more restricted orientation distribution is required, recover forces for the orientation of a fiber have to be included. This could be obtained by forces on the extremities of a fiber. As we included no restrictions in changing the mean fiber orientation

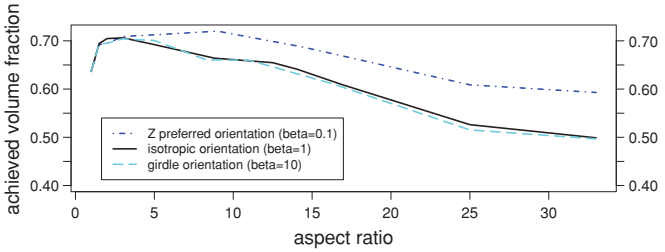

FIG. 7. (Color online) Maximal volume fractions for realizations with varying orientation distributions and aspect ratios.

during the packing process, the system will relax in a less restrictive configuration.

IV. DISCUSSION

In this section, we discuss the volume fractions achieved by numerical simulations and the evolution of the repulsion and recover forces during the fiber packing. Furthermore, we analyze the computing time.

A. Volume fraction

The maximal volume fraction depends on the aspect ratio and on the orientation distribution of the system. Figure 7 shows the maximal volume fractions, achieved with realizations for the β orientation distribution with $\beta \in \{0.1, 1, 10\}$ and varying aspect ratio $\chi \in [1, 33]$. We achieved the highest volume fraction of 72.0075% for an aspect ratio of 9 and a z-axis preferred orientation distribution with $\beta = 0.1$. In general, Fig. 7 supports the intuitive expectation that fibers can be packed in a particularly dense system if they are oriented parallel and that short fibers can be packed more easily.

In Fig. 8, the ratio of achieved volume fraction to initial volume fraction is shown. The initial volume fraction is the sum of all fiber volumes after the random walk divided by the window size. The change of the distances between the balls is related to a change in the volume fraction. As we allow small deviations in the distances, we allow also small deviation in the volume fraction. Here the deviation of the distances is limited to 10%. As a consequence, there also exists a limit for the deviation of the volume fraction caused by the distance change. It ranges from 90% to 110% of the initial volume fraction. Another deviation in the volume fraction is caused by the end step, reducing the radii. The maximal overlap is $0.1 r_{\min}$, and a radius r is maximally reduced by $\frac{1}{2}\text{overlap} \leqslant 0.05 r_{\min} \leqslant 0.05 r$. Therefore, the volume V of a fiber could maximally be reduced to

$$V' \approx l\pi (r')^2 > (0.95)^2 l\pi r^2 \approx 0.9025\, V.$$

Thus, a lower limit for the volume fraction would be $0.9 \times 0.9025 = 81.225\%$ of the initial volume fraction. The upper limit remains at 110% since the radius is not enlarged in the end step. Note that this is a rough approximation of the limits. Particularly for dense systems, it may happen that bending or force-canceling effects influence the structural arrangement, so that these limits are exceeded. This happened in Fig. 8 for the point with the highest required volume fraction of 90%, which is impossible to reach for a fiber system.

The reduction of the volume fraction is expected for dense systems of fibers with a low aspect ratio, where the packing consists of moving and shortening of the objects, which causes a decrease of the volume fraction. The aspect ratio 1 is a special case, as the "fibers" consist only of one ball and shortening is not possible. For a high aspect ratio, the packing is essentially bending the fibers around each other, which causes elongation of the fibers and rising of the volume fraction.

B. Evolution of forces

Figure 9 shows the evolution of the repulsion and recover forces during the fiber packing. Initially, the recover force is zero, as the fibers still have the initial structure, whereas the repulsion force is high at the beginning because the fibers can overlap without restriction. The repulsion force is decreasing very quickly, while the recover force rises slightly in the first steps, caused by the displacements according to the repulsion forces, and decreases quite smoothly with respect to the parameter ρ.

C. Computing time

In practical applications the algorithm showed good performance. All time measurements are taken with a desktop

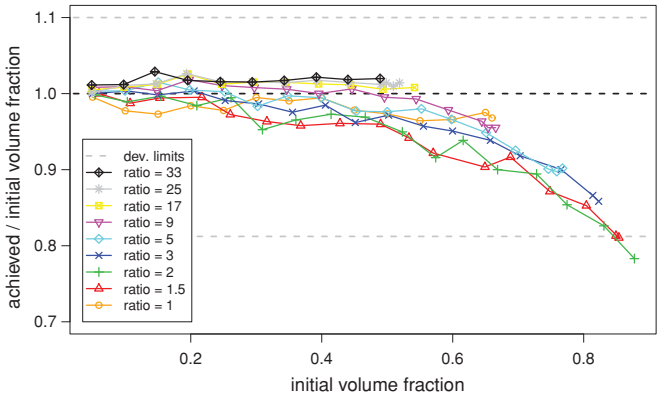

FIG. 8. (Color online) Ratio of the achieved volume fraction and the initial volume fraction for isotropic orientation distribution.

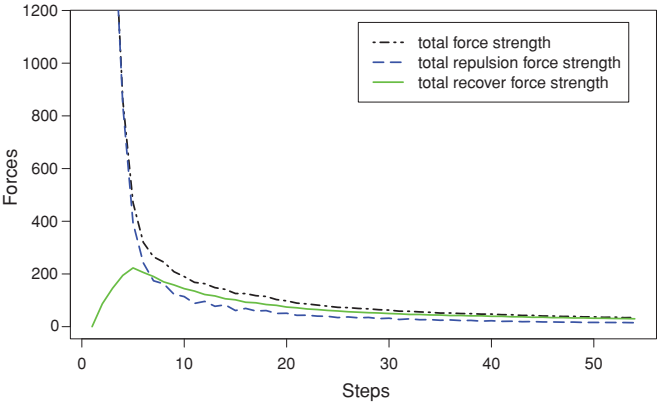

FIG. 9. (Color online) Evolution of force during the fiber packing process. Aspect ratio $\chi = 6$. Isotropic orientation distribution.

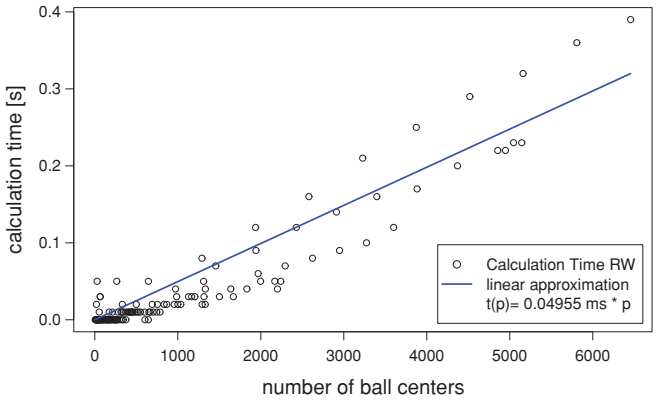

(a) Computing time of random walk vs. amount of ball centers.

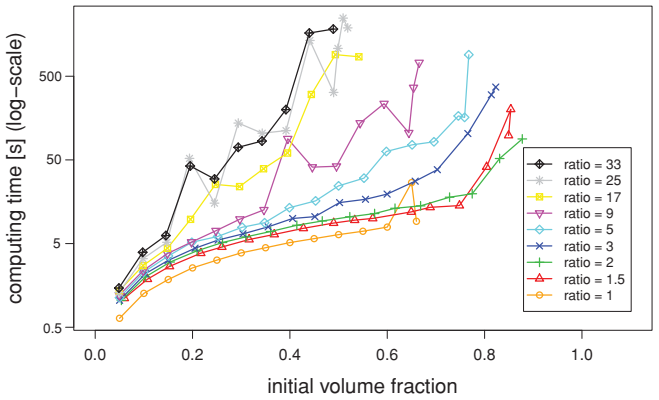

(b) Computing time of fiber packing vs. initial volume fraction.

FIG. 10. (Color online) Computing time of the random walk and the fiber packing for isotropic orientation distribution and constant fiber volume of $0.005s^3$, with $s = 100$ window side length.

PC with an Intel(R) Core(TM)2 processor with CPU X6800, 2.93 GHz, and 3.8 GB memory. The creation time for the random walk progresses approximately linearly with the number of steps, which corresponds to the total number of ball centers in the system. The mean creation time per ball center is approximately 0.05 ms:

$$t_{\mathrm{RW}} \approx 0.05 \text{ ms} \times \text{number of ball centers}.$$

The computing time for the fiber packing increases exponentially with the volume fraction V_V for a fixed aspect ratio χ. This is caused by the enormous increase in interaction with increasing volume fraction. Still, the realization with the longest computing time took about 41 min for an aspect ratio $\chi = 25$, an isotropic orientation distribution, and an achieved volume fraction of $V_V = 51.43\%$, which is at the limit of the possible volume fraction for the given parameters. The computing time is acceptable for those circumstances and a standard desktop computer. The computing time for the random walk and the fiber packing are shown in Fig. 10.

V. CONCLUSION AND PERSPECTIVES

We have presented an algorithm generating bending hard-core fibers, with given orientation, radius, and length distributions. We showed how to evaluate the quality of the final configuration of the fiber system. For the performed realization we could achieve high convergence to the requested parameters, and for the global orientation distribution, we studied the realizable range for the parameter β. In the furure, we will include further recover forces to be able to realize more restricted orientation distributions.

In practical tests, we achieved the highest volume fraction of 72.0075% for the β orientation distribution ($\beta = 0.1$) and an aspect ratio of 9. Practical applications for isotropic orientation distribution have shown a computing time linearly dependent on the number of points for the random walk and a computing time exponentially increasing with the initial volume fraction for the fiber packing.

A soft-shell ratio can be easily included to allow partial overlap or to keep distances between the objects. In the overlap calculation, each radius would be multiplied by the soft-shell ratio. Further studies will include the observation of additional morphological properties during the packing process and the application and adaption of the model parameters to data sets on real materials.

ACKNOWLEDGMENTS

We thank Professor Joachim Ohser, who came up with the idea of applying the force-biased approach to fibers. We also thank Dr. Oliver Wirjadi for the implementation of the VTK SURFACE LABEL RENDERING, which provided us with the shown visualizations. This work is financially supported by the Institute Carnot M.I.N.E.S. and Fraunhofer ITWM, Kaiserslautern. The authors are grateful to the reviewers for helping to improve the first version of the paper.

[1] G. Matheron, *Random Sets and Integral Geometry*, Wiley Series in Probability and Mathematical Statistics (Wiley, New York, 1974).
[2] B. Widom, J. Chem. Phys. **44**, 3888 (1966).
[3] J. Feder, J. Theor. Biol. **87**, 237 (1980).
[4] A. Bezrukov and D. Stoyan, Part. Part. Syst. Charact. **23**, 388 (2006).
[5] S. R. Williams and A. P. Philipse, Phys. Rev. E **67**, 051301 (2003).
[6] N. Provatas, M. Haataja, J. Asikainen, S. Majaniemi, M. Alava, and T. Ala-Nissila, Colloids Surf. A **165**, 209 (2000).
[7] D. Coelho, J.-F. Thovert, and P. M. Adler, Phys. Rev. E **55**, 1959 (1997).
[8] Y. Pan, L. Iorga, and A. A. Pelegri, Compos. Sci. Technol. **68**, 2792 (2008).
[9] O. Wirjadi, Ph.D. thesis, Technische Universität Kaiserslautern, 2009.
[10] S. Karkkainen, J. Nyblom, A. Miettinen, T. Turpeinen, and P. Pötschke (unpublihsed) [http://newrobin.mat.unimi.it/OCS/index.php/ECS/ecs10/paper/view/62].
[11] M. Faessel, C. Delisée, F. Boss, and P. Castera, Compo. Sci. Technol. **65**, 1931 (2005).

[12] N. C. Karayiannis and M. Laso, Macromolecules **41**, 1537 (2008).
[13] K. Schulgasser, J. Mater. Sci. **20**, 859 (1985).
[14] W.-K. Chin, H.-T. Liu, and Y.-D. Lee, Polymer Compos. **9**, 27 (1988).
[15] L. Jain and R. Wetherhold, Acta Metall. Mater. **40**, 1135 (1992).
[16] P. J. Hine, N. Davidson, R. A. Duckett, and I. M. Ward, Compos. Sci. Technol. **53**, 125 (1995).
[17] S.-Y. Fu and B. Lauke, Compos. Sci. Technol. **56**, 1179 (1996).
[18] V. Favier, R. Dendievel, G. Canova, J. Cavaille, and P. Gilormini, Acta Mater. **45**, 1557 (1997).
[19] L. Berhan and A. M. Sastry, Phys. Rev. E **75**, 041120 (2007).
[20] L. Berhan and A. M. Sastry, Phys. Rev. E **75**, 041121 (2007).
[21] H. Altendorf and D. Jeulin, Image Anal. Stereol. **28**, 143 (2009).
[22] H. Altendorf and D. Jeulin, in *ISMM 2009 Abstract Book*, edited by M. H. F. Wilkinson and J. B. T. M. Roerdink (University of Groningen, Groningen, The Netherlands, 2009), pp. 33–36.
[23] G. Cinacchi and L. D. Gaetani, Phys. Rev. E **77**, 051705 (2008).
[24] J. Mościński and M. Bargieł, Mol. Simul. **3**, 201 (1989).
[25] A. Bezrukov, M. Bargieł, and D. Stoyan, Part. Part. Syst. Charact. **19**, 111 (2002).
[26] M. Laso, N. C. Karayiannis, K. Foteinopoulou, M. L. Mansfield, and M. Kröger, Soft Matter. **5**, 1762 (2009).
[27] E. L. Hinrichsen, J. Feder, and T. Jøssang, Phys. Rev. A **41**, 4199 (1990).
[28] K. Schladitz, S. Peters, D. Reinel-Bitzer, A. Wiegmann, and J. Ohser, Comput. Mater. Sci. **38**, 56 (2006).
[29] J. Ohser and K. Schladitz, *3D Images of Materials Structures: Processing and Analysis* (Wiley-VCH, Weinheim, Germany, 2009).
[30] N. I. Fisher, B. J. J. Embleton, and T. Lewis, *Statistical Analysis of Spherical Data*, rev. ed. (Cambridge University Press, Cambridge, 1993).